Title
THE STEADY LAMINAR FLOW PAST A CIRCULAR CYLINDER

Authors
McDonald, Marvin E.
Newman, John.

Publication Date
1967-02-01

UCRL-17374

University of California

Ernest O. Lawrence Radiation Laboratory

THE STEADY LAMINAR FLOW PAST A CIRCULAR CYLINDER

Berkeley, California

DISCLAIMER

Submitted to American Institute
of Chemical Engineers J.

UCRL-17374
Preprint

UNIVERSITY OF CALIFORNIA

Lawrence Radiation Laboratory
Berkeley, California

AEC Contract W-7405-eng-48

THE STEADY LAMINAR FLOW PAST A CIRCULAR CYLINDER

Marvin E. McDonald and John Newman

February, 1967

The Steady Laminar Flow past a Circular Cylinder

Marvin E. McDonald and John Newman

Inorganic Materials Research Division,
Lawrence Radiation Laboratory, and
Department of Chemical Engineering
University of California, Berkeley

February, 1967

Abstract

A regular perturbation solution of the Navier-Stokes equations is presented and applied to the circular cylinder in transverse flow.

At a Reynolds number of 300, results for the first perturbation show a secondary vortex near the rear stagnation point and a wake stagnation point located at $r = 5.14$. The experimental data of Grove[3] and existing numerical solutions for $Re \leq 40$ indicate that more terms of the series are needed to describe the flow accurately.

1. Introduction

Problems in fluid mechanics are governed by nonlinear partial differential equations. Exact solutions of these equations are rare, and many times one must resort to approximations such as singular perturbation expansions or numerical solutions. For flow past bluff bodies, separation occurs at high Reynolds numbers. Singular perturbation techniques have not been very successful for these separated flows because the correct limiting solution for $Re \to \infty$ is not known.

A different approach[9] recognizes that the potential flow past an object is an exact solution of the Navier-Stokes equations at any Reynolds number if a slip velocity which conforms to the potential flow is prescribed on the object's surface. A perturbation of this surface boundary condition generates a regular perturbation solution - i.e., one that is uniformly valid. The perturbation procedure is not a perturbation in the Reynolds number - it is an expansion with the Reynolds number fixed.

The linearized problem is still sufficiently complex for numerical techniques to be used. The first correction to the potential flow of a Newtonian fluid past a circular cylinder has been computed for a Reynolds number of 300.[8] The flow is assumed to be laminar and steady, and the density and viscosity are constant. Actually the flow past a circular cylinder becomes unsteady at a Reynolds number of about 40; but, the steady flow can be found by requiring a plane of symmetry.

Many other investigators have done theoretical work on flow past cylinders in this range of the Reynolds number where both viscous and inertial forces are important. Some of these are Apelt[2], Allen and Southwell[1] and Sih[10].

2. Problem Statement

a. Mathematical Formulation

The problem may be formulated in terms of the vorticity transport equation

$$\frac{\partial \psi^*}{\partial y^*}\frac{\partial \omega^*}{\partial x^*} - \frac{\partial \psi^*}{\partial x^*}\frac{\partial \omega^*}{\partial y^*} = \nu\left(\frac{\partial^2 \omega^*}{\partial x^{*2}} + \frac{\partial^2 \omega^*}{\partial y^{*2}}\right), \tag{2.1}$$

where ν is the constant kinematic viscosity of the fluid. The stream function ψ^* and vorticity ω^* are related by Poisson's equation

$$\frac{\partial^2 \psi^*}{\partial x^{*2}} + \frac{\partial^2 \psi^*}{\partial y^{*2}} = -\omega^* . \tag{2.2}$$

The velocity components may be obtained from the definition of the stream function

$$v_x^* = \frac{\partial \psi^*}{\partial y^*} \quad \text{and} \quad v_y^* = -\frac{\partial \psi^*}{\partial x^*}, \tag{2.3}$$

and the vorticity is related to the velocity by

$$\omega^* = \frac{\partial v_y^*}{\partial x^*} - \frac{\partial v_x^*}{\partial y^*} . \tag{2.4}$$

The circular cylinder and coordinate systems are shown in Figure 1.

The boundary conditions are

$$\frac{\partial \psi^*}{\partial x^*} \to 0, \quad \frac{\partial \psi^*}{\partial y^*} \to U, \quad \omega^* \to 0 \text{ as } r^* \to \infty , \tag{2.5}$$

$$\frac{\partial \psi^*}{\partial \theta} = 0 \text{ at } r^* = R , \tag{2.6}$$

$$\frac{\partial \psi^*}{\partial r^*} = 2U(1-\epsilon)\sin\theta \text{ at } r^* = R , \tag{2.7}$$

$$\psi^* = 0 \text{ at } r^* = R , \tag{2.8}$$

$$\psi^* = 0 \text{ for } |x^*| > R,\ y^* = 0, \text{ and} \tag{2.9}$$

$$\omega^* = 0 \text{ for } |x^*| > R,\ y^* = 0 . \tag{2.10}$$

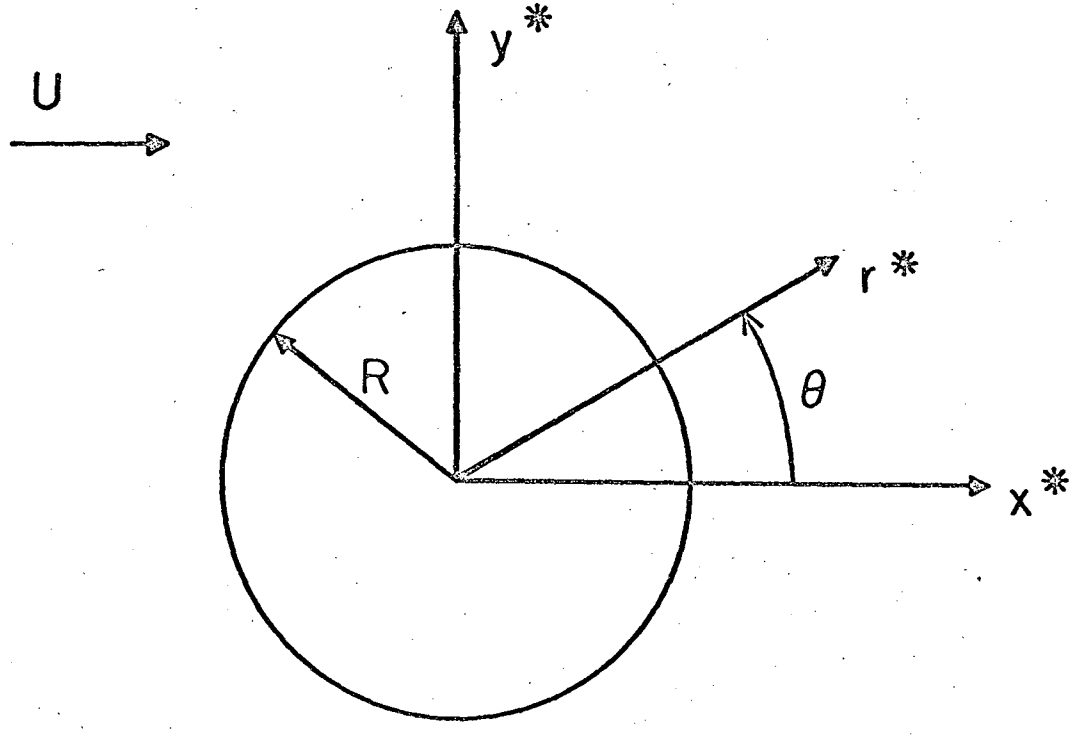

MUB-11488

Figure 1. Coordinate systems for the circular cylinder.

Conditions (2.5) state that the uniform flow is approached far from the cylinder. The vanishing of the tangential gradient of the stream function at the surface of the cylinder, condition (2.6), is necessary to specify zero fluid velocity in the direction normal to the surface. Condition (2.7) describes the slip velocity on the cylinder surface in terms of the parameter ϵ. This parameter is inserted in order to obtain an exact solution to the problem when $\epsilon = 0$. This solution is the potential flow pertinent to the system. Of physical significance is the case $\epsilon = 1$ which gives a zero tangential velocity at the cylinder surface. This work is restricted to flows which are symmetric to the x^*-axis, which necessitates conditions (2.8), (2.9), and (2.10).

It is convenient to work with dimensionless variables. Let

$$\left.\begin{aligned} &y = y^*/R,\ x = x^*/R,\ r = r^*/R,\ \delta = \nu/UR = 2/Re\ , \\ &\omega = R\omega^*/U,\ \psi = \psi^*/UR,\ P = (p-p_\infty)/\tfrac{1}{2}\rho U^2,\ m = D/\rho U^2 R\ . \end{aligned}\right\} \quad (2.11)$$

Equations (2.1) and (2.2) become

$$\delta\left(\frac{\partial^2\omega}{\partial x^2} + \frac{\partial^2\omega}{\partial y^2}\right) = \frac{\partial\psi}{\partial y}\frac{\partial\omega}{\partial x} - \frac{\partial\psi}{\partial x}\frac{\partial\omega}{\partial y} \quad (2.12)$$

and

$$\frac{\partial^2\psi}{\partial x^2} + \frac{\partial^2\psi}{\partial y^2} = -\omega\ . \quad (2.13)$$

After a conformal transformation to new independent variables, α and β, these equations are

$$\delta\left(\frac{\partial^2\omega}{\partial\alpha^2} + \frac{\partial^2\omega}{\partial\beta^2}\right) = \frac{\partial\psi}{\partial\beta}\frac{\partial\omega}{\partial\alpha} - \frac{\partial\psi}{\partial\alpha}\frac{\partial\omega}{\partial\beta} \quad (2.14)$$

and

$$h^2\left(\frac{\partial^2\psi}{\partial\alpha^2} + \frac{\partial^2\psi}{\partial\beta^2}\right) = -\omega\ . \quad (2.15)$$

The new coordinates α and β are, respectively, the dimensionless

velocity potential and stream function which are the solutions to the problem when $\epsilon = 0$. These coordinates are related to x and y by

$$\alpha = x(1 + 1/r^2) \tag{2.16}$$

$$\text{and} \quad \beta = y(1 - 1/r^2) \, . \tag{2.17}$$

It is advantageous that in the α, β plane, the cylinder is a straight line on the α-axis. The front and rear stagnation points correspond to $\alpha = -2$ and $\alpha = +2$, respectively.

The square of the magnitude of the potential flow velocity is h^2, and it can be readily shown that

$$h^2 = (1 + 1/r^2)^2 - 4\alpha^2/(r^2 + 1)^2 \, . \tag{2.18}$$

It is desirable to express h^2 explicitly in terms of α and β, and the necessary relationship is

$$r = \tfrac{1}{4}\left\{\sqrt{(\alpha-2)^2+\beta^2} + \sqrt{(\alpha+2)^2+\beta^2} + \sqrt{2}\left[\sqrt{(\alpha-2)^2+\beta^2}\,\sqrt{(\alpha+2)^2+\beta^2} + (\alpha-2)(\alpha+2) + \beta^2\right]^{\frac{1}{2}}\right\} . \tag{2.19}$$

The behavior of h^2 on the cylinder surface and near the stagnation points is given by

$$h^2(\alpha,0) = 4 - \alpha^2, \quad |\alpha| \leq 2 \, , \tag{2.20}$$

$$h^2(\alpha,\beta) \to 4\sqrt{(2-\alpha)^2+\beta^2} \text{ as } \alpha \to +2, \ \beta \to 0 \, , \tag{2.21}$$

$$h^2(\alpha,\beta) \to 4\sqrt{(2+\alpha)^2+\beta^2} \text{ as } \alpha \to -2, \ \beta \to 0 \, . \tag{2.22}$$

b. Perturbation Approach

All dependent variables are expanded in power series in ϵ,

$$\psi = \beta + \epsilon \, \psi^{(1)} + \epsilon^2 \, \psi^{(2)} + \ldots \tag{2.23}$$

$$\omega = \epsilon \, \omega^{(1)} + \epsilon^2 \, \omega^{(2)} + \ldots \, , \tag{2.24}$$

etc. The zero order perturbation terms are $\psi^{(0)} = \beta$ and $\omega^{(0)} = 0$. The differential equations for the higher perturbations are

$$\delta\left(\frac{\partial^2\omega^{(n)}}{\partial\alpha^2} + \frac{\partial^2\omega^{(n)}}{\partial\beta^2}\right) = \frac{\partial\omega^{(n)}}{\partial\alpha} + f^{(n)}(\alpha,\beta) \tag{2.25}$$

$$h^2\left(\frac{\partial^2\psi^{(n)}}{\partial\alpha^2} + \frac{\partial^2\psi^{(n)}}{\partial\beta^2}\right) = -\omega^{(n)},\ n = 1,2,\ldots, \tag{2.26}$$

where

$$f^{(1)}(\alpha,\beta) = 0\ , \tag{2.27}$$

$$f^{(2)}(\alpha,\beta) = \frac{\partial\psi^{(1)}}{\partial\beta}\frac{\partial\omega^{(1)}}{\partial\alpha} - \frac{\partial\psi^{(1)}}{\partial\alpha}\frac{\partial\omega^{(1)}}{\partial\beta}\ , \tag{2.28}$$

etc. The boundary conditions are

$$\psi^{(n)} = 0 \text{ at } \beta = 0,\ n = 1,2,\ldots, \tag{2.29}$$

$$\frac{\partial\psi^{(1)}}{\partial\beta} = -1,\ \frac{\partial\psi^{(n)}}{\partial\beta} = 0,\ n = 2,3,\ldots, \text{ at } \beta = 0,\ |\alpha| \le 2 \tag{2.30}$$

$$\frac{\partial^2\psi^{(n)}}{\partial\beta^2} = 0\ ,\ \omega^{(n)} = 0 \text{ at } \beta = 0,\ |\alpha| > 2,\ n = 1,2,\ldots, \tag{2.31}$$

$$\frac{\partial\psi^{(n)}}{\partial\alpha} \to 0\ ,\ \frac{\partial\psi^{(n)}}{\partial\beta} \to 0\ ,\ \omega^{(n)} \to 0 \text{ as } \alpha^2 + \beta^2 \to \infty\ ,\ n = 1,2,\ldots \tag{2.32}$$

The primary advantage of the α,β coordinate system is that equation (2.25) has the same form as the Oseen equation in rectangular coordinates.

c. Solution of the Equations

In the later sections, the first perturbation only is considered. In view of this, the solution is given for n = 1 only. Southwell and Squire[11] have obtained the solution to the first perturbation also. They calculated results for a Reynolds number of 2. The solution can be extended to higher perturbations, but the analysis becomes more complicated.

The solution to equation (2.25) for the first perturbation is

$$\omega^{(1)}(\alpha,\beta) = \frac{\beta}{2\pi\delta}\int_{-2}^{+2} \frac{\sigma^{(1)}(\tau)e^{\frac{\alpha-\tau}{2\delta}} K_1\left(\sqrt{\left(\frac{\alpha-\tau}{2\delta}\right)^2 + \left(\frac{\beta}{2\delta}\right)^2}\right)}{\sqrt{(\alpha-\tau)^2+\beta^2}}\, d\tau \,, \tag{2.33}$$

where $\sigma^{(1)}(\tau)$ is the unknown surface vorticity for the first perturbation and $K_1(r)$ is the modified Bessel function of the second kind or order 1.

The solution to equation (2.26) for n = 1 is

$$\psi^{(1)}(\alpha,\beta) = -\frac{1}{2\pi}\int_{-\infty}^{+\infty}\int \frac{\omega^{(1)}(a,b)}{h^2(a,b)} \ln\sqrt{(\alpha-a)^2+(\beta-b)^2}\; da\, db \,. \tag{2.34}$$

The remaining boundary condition, $\frac{\partial\psi^{(1)}}{\partial\beta} = -1$ at $\beta = 0$, $|\alpha| < 2$ yields an integral equation for $\sigma^{(1)}(\tau)$,

$$-2\pi = \int_{-2}^{+2} \sigma^{(1)}(\tau)\, K(\alpha,\tau)\, d\tau \,, \tag{2.35}$$

where the kernel is given by

$$K(\alpha,\tau) = \frac{1}{\pi}\int_{-\infty}^{+\infty}\int \frac{F\left(\frac{a-\tau}{2\delta}, \frac{b}{2\delta}\right)}{h^2(a,b)[(\alpha-a)^2+b^2]}\; da\, db \,, \tag{2.36}$$

with

$$F(A,B) = \frac{B^2 e^A K_1\left(\sqrt{A^2+B^2}\right)}{\sqrt{A^2+B^2}} \,. \tag{2.37}$$

The drag coefficient and pressure correction at the rear stagnation point for the first perturbation can also be obtained. These are

$$m^{(1)} = -2\delta\int_{-2}^{+2} \sigma^{(1)}(\tau)\, d\tau \,, \tag{2.38}$$

and

$$P^{(1)}(2,0) = \frac{1}{\pi}\int_{-2}^{+2} \sigma^{(1)}(\tau) e^{\frac{2-\tau}{2\delta}}\left[K_0\left(\frac{2-\tau}{2\delta}\right) + K_1\left(\frac{2-\tau}{2\delta}\right)\right] d\tau \,. \tag{2.39}$$

3. Outline of Numerical Solution

The numerical solution centers around the calculation of $\sigma^{(1)}(\alpha)$ from equation (2.35). This is not an easy matter because the kernel of the integral equation is difficult to evaluate.

After $\sigma^{(1)}(\alpha)$ has been obtained, $m^{(1)}$ and $P^{(1)}(2,0)$ are easily obtained from equations (2.38) and (2.39). Next $\omega^{(1)}(\alpha,\beta)$ follows by quadrature from equation (2.33). Finally, $\psi^{(1)}(\alpha,\beta)$ could be obtained from equation (2.34), but it is much simpler to solve equation (2.26) by finite difference methods.

In essence, one avoids the numerical solution of a fourth order partial differential equation for $\psi^{(1)}$ by using instead the integral equation to obtain the surface vorticity.

4. Kernel

The solution of equation (2.35) as shown in section 5 requires the evaluation of $K(\alpha,\tau)$ a large number of times. Thus, an efficient procedure is desired for this evaluation. First a discussion is given on the behavior of the kernel, and then we turn to its evaluation.

a. Properties of the Kernel

Figure 2 is a plot of $K(0.0775,\tau)$ versus τ for a Reynolds number of 300. From this figure some of the general features may be deduced. These properties can also be inferred from equation (2.36). It is seen that $K(\alpha,\tau)$ is infinite for $\alpha=\tau$ and the function is greater for $\alpha > \tau$ than for $\alpha < \tau$. The way in which $K(\alpha,\tau)$ becomes infinite may be obtained from the flat plate kernel.

For a flat plate, $h^2(a,b) \equiv 1$ and the kernel for this case is

$$K(\alpha,\tau) = \frac{1}{\pi}\int_{-\infty}^{+\infty}\int \frac{F\left(\frac{a-\tau}{2\delta}, \frac{b}{2\delta}\right)}{[(\alpha-a)^2+b^2]}\,da\,db = e^{\eta}[K_0(|\eta|) + \mathrm{sgn}(\eta)\,K_1(|\eta|)] - \frac{1}{\eta} \quad (4.1)$$

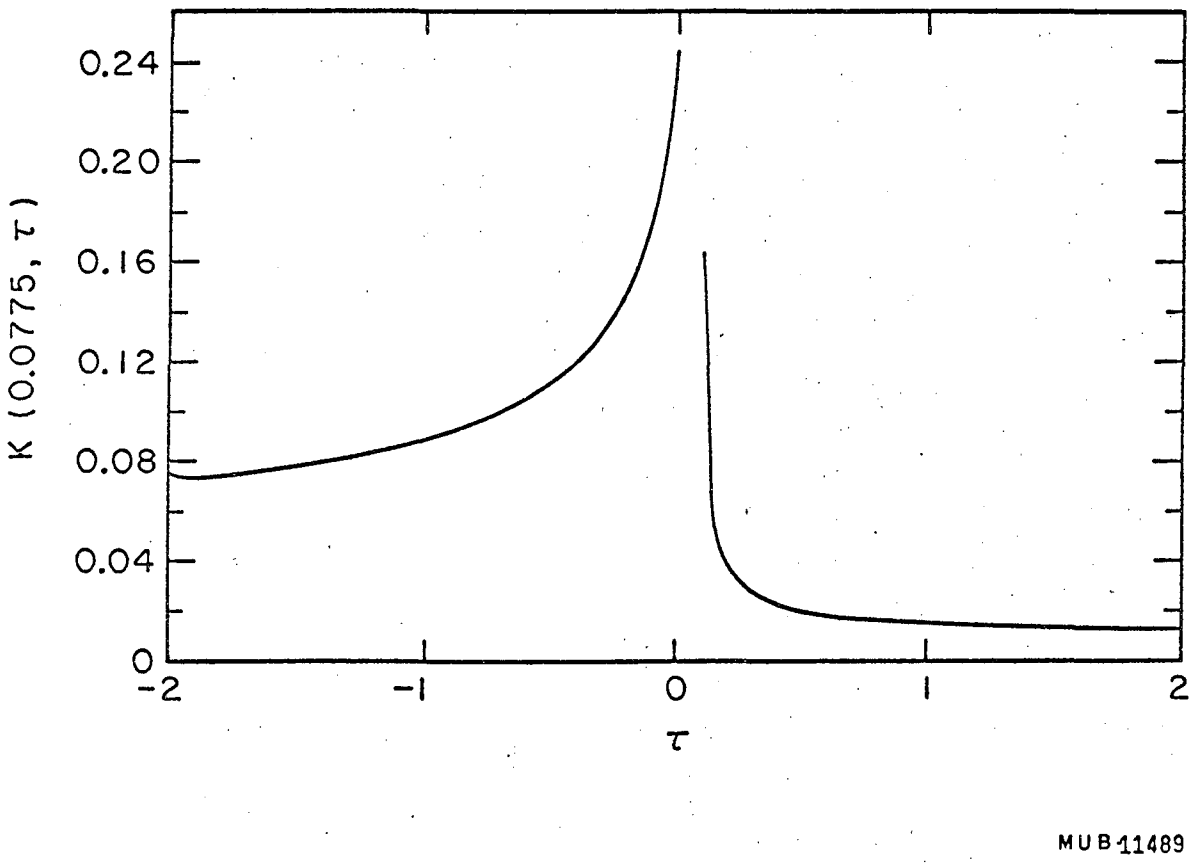

Figure 2. Kernel for $\alpha = 0.0775$ and a Reynolds number of 300.

where $\eta = \frac{\alpha-\tau}{2\delta}$ and sgn(η) is the sign (+1 or -1) of η. For further reference, denote

$$\chi(\alpha,\tau) = \frac{e^{\eta}[K_o(|\eta|) + \text{sgn}(\eta)\, K_1(|\eta|)] - \frac{1}{\eta}}{h^2(\alpha,0)} \quad . \tag{4.2}$$

The flat plate kernel is important because it shows the form of the singularity of $K(\alpha,\tau)$. As $\tau \to \alpha$, the major contribution to the integral in equation (2.36) comes from a small region surrounding $a = \alpha$, $b = 0$. Thus,

$$K(\alpha,\tau) \to \chi(\alpha,\tau) \text{ as } \tau \to \alpha, \ |\alpha| \neq 2 \ , \tag{4.3}$$

where the stagnation points have been excluded because $h^2(\alpha,0)$ is zero at these points. Recalling that $K_o(|\eta|) \to -\ln \frac{|\eta|}{2}$ and $K_1(|\eta|) \to \frac{1}{|\eta|}$ as $\eta \to 0$, equation (4.3) becomes

$$K(\alpha,\tau) \to \frac{-\ln \left|\frac{\alpha-\tau}{4\delta}\right|}{h^2(\alpha,0)} \text{ as } \tau \to \alpha, \ |\alpha| \neq 2. \tag{4.4}$$

It is evident upon further examination that $\chi(\alpha,\tau)$ behaves very similarly to $K(\alpha,\tau)$ for all τ so long as $|\alpha| \neq 2$. This proves useful in the solution of the integral equation for the cylinder.

b. Numerical Evaluation of the Kernel

The kernel is to be calculated for various values of α and τ ranging from -2 to +2 at a Reynolds number of 300 ($\delta = 2/300$). Equation (2.36) can be rewritten as twice the integral over the upper half plane.

$$K(\alpha,\tau) = \frac{2}{\pi} \int_0^{+\infty} \int_{-\infty}^{+\infty} G(A,B)\, dA\, dB \ , \tag{4.5}$$

where,

$$G(A,B) = \frac{B^2 e^A K_1\left(\sqrt{A^2+B^2}\right)}{h^2(2\delta A+\tau, 2\delta B)\left[\left(A - \frac{\alpha-\tau}{2\delta}\right)^2 + B^2\right]\sqrt{A^2+B^2}} \ . \tag{4.6}$$

The variables of integration have been changed to $A = \frac{a-\tau}{2\delta}$ and $B = \frac{b}{2\delta}$.

It is advantageous to use these new variables when the Reynolds number is large.

In any numerical integration, the behavior of the integrand must be accounted for. Here, the problem is difficult because G(A,B) has several peculiarities to contend with. When $\alpha=\tau$, G(A,B) is infinite at the point A=0, B=0, and the integral diverges at this point. The kernel is finite for all other values of α and τ, but some singular behavior is present in G(A,B) for all values of α and τ.

When $\tau \neq \alpha$, G(A,B) is zero on the B axis except for A=0, $|\tau| \neq 2$ and $A = \frac{\alpha-\tau}{2\delta}$, $|\alpha| \neq 2$ where it is finite. When $|\tau| = 2$, $G(A,B) \to \infty$ as $A \to 0$, $B \to 0$, and when $|\alpha| = 2$, $G(A,B) \to \infty$ as $A \to \frac{\alpha-\tau}{2\delta}$, $B \to 0$. Thus, regions surrounding these points require special consideration. Actually, owing to the method of solving the integral equation, the points $|\alpha| = 2$ and $|\tau| = 2$ do not have to be considered. Of course the integrand approaches this singular behavior when α or τ is near a stagnation point.

To evaluate the kernel, the upper half plane is divided into a number of regions. The way in which it is divided is dependent upon the location of α and τ relative to each other and relative to the stagnation points. The method used in this work divides the upper half plane in twenty different ways depending on the location of α and τ. To illustrate the method the procedure for calculating K(1.98,-1.0) will be given. Figure 3 shows how the total integration region is divided. Regions 1, 2, 3, 6, 7, 8 and 10 extend to infinity in the B direction, and regions 1 and 10 extend to infinity in the +A and -A directions, respectively. The constants which define the regions, for these particular values of α and τ, are A_1=-2, A_2=2, A_3=221.5, A_4=224.5, A_5=227, A_6=300, and $B_1 \doteq 0.5$. The front stagnation point corresponds to $A = \frac{-2-\tau}{2\delta} = -75$, and the rear stagnation point $A = \frac{2-\tau}{2\delta} = 225$. The rear

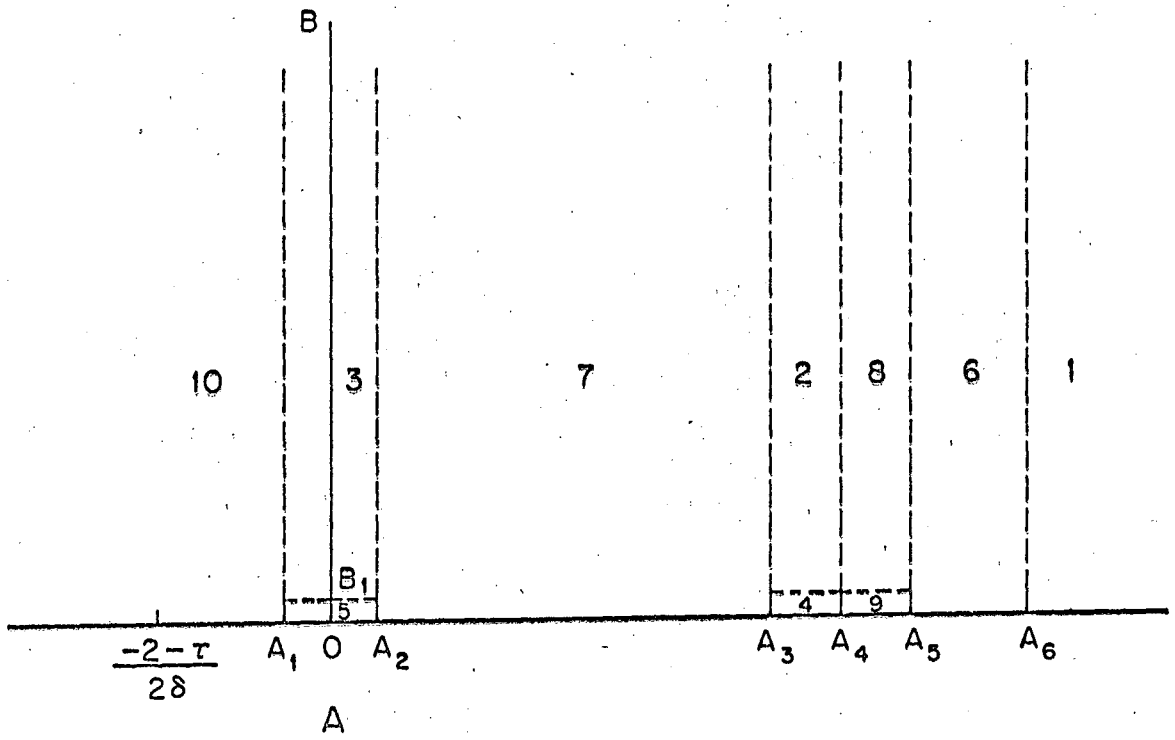

Figure 3. Division of the upper half plane (not to scale).

stagnation point is in region 9. Region 4 includes the point $A = \frac{\alpha-\tau}{2\delta} = 223.5$.

To perform the necessary quadratures, Gauss-Laguerre and Gauss-Legendre quadrature formulas are applied. When the integration interval is finite, the 5-point Gauss-Legendre formula is used with subintervals. When the upper limit of integration extends to infinity, the Gauss-Laguerre quadrature formula (up to 32 points) is usually used. Quadrature formulas of the Gaussian type are discussed in most texts on numerical analysis, including Krylov[6].

Regions 2, 3, 6, 7 and 8 cause no special problems. The Gauss-Laguerre formula is applied in the B direction and the Gauss-Legendre formula in the A direction.

In region 1, the behavior of G(A,B) does not permit the application of the Gauss-Laguerre formula in either direction. Variable transformations $C = \ln A$ and $D = \frac{B}{\sqrt{2A}}$ rectify the situation. The Gauss-Laguerre formula can then be applied in the C direction. The integrand is very small for $D > 5$, and all significant contribution is contained within D=5. Thus, between D=0 and D=5, the Gauss-Legendre formula is appropriate.

Region 4 surrounds the point $A = \frac{\alpha-\tau}{2\delta}$, B=0, and region 5 surrounds the point A=0, B=0. The integrand behaves similarly in these two regions, and the integration is conducted in very nearly the same manner for the two. Hence, the procedure is illustrated for region 5 only. When $A \to 0$ and $B \to 0$ the integrand is badly behaved. When the argument of the Bessel function is small

$$G(A,B) \to \frac{1}{h^2(\tau,0)\left(\frac{\alpha-\tau}{2\delta}\right)^2} \frac{B^2}{A^2+B^2} \cdot \tag{4.7}$$

The worst of the behavior can be subtracted from the integrand to obtain,

for region 5,

$$I = \frac{2}{\pi} \int_0^{B_1} \int_{A_1}^{A_2} \left[G(A,B) - \frac{1}{h^2(\tau,0)\left(\frac{\alpha-\tau}{2\delta}\right)^2} \frac{B^2}{A^2+B^2} \right] dA\, dB$$

$$+ \frac{2}{\pi h^2(\tau,0)\left(\frac{\alpha-\tau}{2\delta}\right)^2} \int_0^{B_1} \int_{A_1}^{A_2} \frac{B^2}{A^2+B^2}\, dA\, dB \,. \qquad (4.8)$$

The second double integral in equation (4.8) is evaluated analytically, and the first is computed numerically by use of the Gauss-Legendre formula in each direction.

The contribution from region 9 is obtained by applying the Gauss-Legendre formula in each direction. This region contains the rear stagnation point.

In region 10, $G(A,B)$ decreases very fast as $A \to \infty$. The region is further subdivided in the A direction, and the contribution is successively obtained until the contribution is negligible. In the A direction, the Gauss- Legendre formula is used, and in the B direction the Gauss-Laguerre formula is used.

The contribution from each region was calculated to an accuracy of about 0.001 %.

5. Surface Vorticity for the First Perturbation

a. Solution of the Integral Equation

In this section, equation (2.35) is replaced by a system of linear algebraic equations which can then be solved for $\sigma^{(1)}(\alpha)$. The procedure is to approximate the integral equation by a quadrature formula. The formula chosen is the 40-point Gauss-Legendre formula. Some care must be used in doing this because the integral equation is singular. A procedure similar to that proposed by Kantorovich and Krylov[4] is adopted. The surface vorticity

$\sigma^{(1)}(\alpha)$ is to be solved from

$$-2\pi = \int_{-2}^{+2} \sigma^{(1)}(\tau)\, K(\alpha,\tau)\, d\tau \ .$$

The kernel of this equation has a logarithmic singularity at $\alpha=\tau$ as shown by equation (4.4). Hence, a quadrature formula cannot be applied to the equation in its present form.

To the integrand, we add and subtract $\sigma^{(1)}(\alpha)\, \chi(\alpha,\tau)$ where $\chi(\alpha,\tau)$ is undefined for the moment. This yields

$$-2\pi = \int_{-2}^{+2} [\sigma^{(1)}(\tau)\, K(\alpha,\tau) - \sigma^{(1)}(\alpha)\, \chi(\alpha,\tau)]d\tau + \sigma^{(1)}(\alpha)\, g(\alpha) \ , \qquad (5.1)$$

where

$$g(\alpha) = \int_{-2}^{+2} \chi(\alpha,\tau)\, d\tau \ . \qquad (5.2)$$

Kantorovich and Krylov recommend using $\chi(\alpha,\tau) = K(\alpha,\tau)$. The integrand of equation (5.1) is then zero at $\alpha=\tau$; but, the evaluation of equation (5.2) would not be easy. Instead, we set $\chi(\alpha,\tau)$ as in equation (4.2). This would not be satisfactory for $|\alpha| = 2$, because $\chi(\alpha,\tau)$ is infinite at these points. However, the points $|\alpha| = 2$ will not be employed in obtaining the solution of this equation. The integrand in equation (5.1) is then finite at $\alpha=\tau$ and equal to $\sigma^{(1)}(\alpha) \lim_{\tau\to\alpha} [K(\alpha,\tau) - \chi(\alpha,\tau)]$.

The term in brackets at $\alpha=\tau$ is given by

$$D(\alpha) = \frac{2}{\pi} \int_{0}^{\infty}\int_{-\infty}^{+\infty} \left[\frac{1}{h^2(2\delta A+\alpha, 2\delta B)} - \frac{1}{h^2(\alpha,0)}\right] \frac{B^2 e^A K_1\left(\sqrt{A^2+B^2}\right)}{[A^2+B^2]^{3/2}}\, dA\, dB, \qquad (5.3)$$

which was computed by the same methods as was $K(\alpha,\tau)$.

The primary advantage in adopting this procedure is that $g(\alpha)$ can be

determined analytically. The result is for $|\alpha| < 2$,

$$g(\alpha) = 2\delta \left\{ 2\xi_1 e^{\xi_1}[K_o(\xi_1) + K_1(\xi_1)] - e^{\xi_1}K_o(\xi_1) + 2\xi_2 e^{-\xi_2}[K_o(\xi_2) - K_1(\xi_2)] + e^{-\xi_2}K_o(\xi_2) + \ln \xi_2/\xi_1 \right\} \Big/ h^2(\alpha,0) , \quad (5.4)$$

where $\xi_1 = \frac{2+\alpha}{2\delta}$ and $\xi_2 = \frac{2-\alpha}{2\delta}$.

Approximation of the integral in equation (5.1) by the 40-point Gauss-Legendre formula gives

$$-2\pi = \sum_{i=1}^{40} 2H_i[\sigma^{(1)}(\alpha_i)K(\alpha,\alpha_i) - \sigma^{(1)}(\alpha)\chi(\alpha,\alpha_i)] + \sigma^{(1)}(\alpha)g(\alpha) . \quad (5.5)$$

Choosing $\alpha=\alpha_1, \alpha_2, \ldots, \alpha_{40}$ gives 40 simultaneous equations for the determination of $\sigma^{(1)}(\alpha_i)$, which are

$$-2\pi = \sum_{\substack{i=1 \\ i\neq j}}^{40} 2H_i K(\alpha_j,\alpha_i)\sigma^{(1)}(\alpha_i) + \sigma^{(1)}(\alpha_j) \left\{ g(\alpha_j) - \sum_{\substack{i=1 \\ i\neq j}}^{40} 2H_i \chi(\alpha_j,\alpha_i) + 2H_j D(\alpha_j) \right\}, \quad j = 1, 2, \ldots 40 . \quad (5.6)$$

In equation (5.6), $D(\alpha_j)$ is given by equation (5.3).

This system of equations was solved by the Crout elimination method, as given by Lapidus*[7]. Figure 4 shows $\sigma^{(1)}$ plotted versus $2\theta/\pi$, where θ is the angle measured from the rear stagnation point in the x,y plane.

It was felt important to obtain an estimate on the adequacy of representing the integral equation by the 40-point quadrature formula. This check was obtained by resolving equation (5.1) using the 32-point Gauss-Legendre

---

* The equations given by Lapidus for using the Crout elimination method are incorrect.

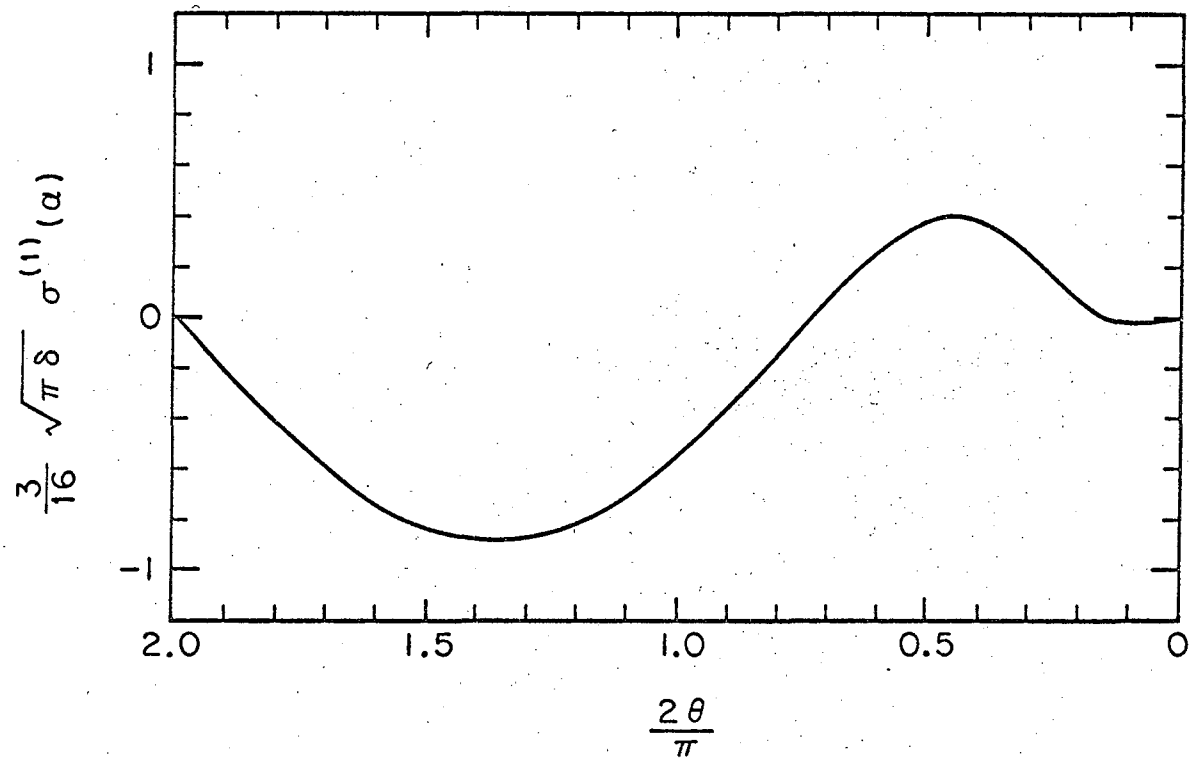

MUB-11491

Figure 4. Surface vorticity for the first perturbation.

formula. The differences in the values of the surface vorticity for n = 32 and n = 40 were less than 1% in most cases. The only exceptions were near the points where $\sigma^{(1)}(\alpha) \to 0$ where the percentage deviation was higher. It is felt that this higher deviation is not important.

b. Interpolation of $\sigma^{(1)}(\alpha)$

The 40 points at which $\sigma^{(1)}(\alpha)$ is known, from the solution of the integral equation, are not sufficient for the calculation of $\omega^{(1)}$ and $p^{(1)}(2,0)$. Thus, interpolation must be used. Use of Lagrange's interpolation formula with the 42 unevenly spaced points at which $\sigma^{(1)}(\alpha)$ is known (40 points from the solution of the integral equation plus the two stagnation points where $\sigma^{(1)}(\alpha) = 0$), results in

$$\sigma^{(1)}(\alpha) = \sum_{i=2}^{41} \prod_{\substack{j=1 \\ j\neq i}}^{42} \frac{\alpha-\alpha_j}{\alpha_i-\alpha_j} \sigma^{(1)}(\alpha_i) . \tag{5.7}$$

The points i = 1 and i = 42 (the stagnation points) have been exluded from the summation because the vorticity is zero at these points.

Equation (5.7) was used to calculate $\sigma^{(1)}(\alpha)$ at 801 equally spaced points in the interval $-2 \leq \alpha \leq 2$, corresponding to a spacing of 0.005. These values were stored on magnetic tape so they could be used in conjunction with Newton's interpolation formulas to calculate $\sigma^{(1)}(\alpha)$ at the points necessary for the determination of $\omega^{(1)}$, $p^{(1)}(2,0)$ and $m^{(1)}$.

6. Drag Coefficient and Pressure Correction

The drag coefficient was calculated by employing the 40-point Gauss-Legendre formula to subintervals. Equation (2.38) becomes

$$m^{(1)} = -2\delta \sum_{k=1}^{n} \int_{-2+(k-1)\ell}^{-2+k\ell} \sigma^{(1)}(\tau)d\tau = -\delta\ell \sum_{k=1}^{n} \int_{-1}^{+1} \sigma^{(1)}\left[\frac{\ell}{2}(z+2k-1)-2\right] dz$$

$$= -\delta\ell \sum_{k=1}^{n} \sum_{i=1}^{40} H_i \sigma^{(1)} \left[\frac{\ell}{2} (z_i+2k-1) -2\right] . \qquad (6.1)$$

In equation (6.1) ℓ is the subinterval length, n is the number of subintervals, H_i and z_i are the Gaussian weights and nodes for the 40-point Gauss-Legendre formula. The result is, with two subintervals, $m^{(1)} = 0.7070$. One subinterval gave the same result to four significant figures.

A completely analogous procedure for the pressure correction gives $P^{(1)}(2,0) = -2.192$.

7. Vorticity for the First Perturbation

The expression for $\omega^{(1)}(\alpha,\beta)$, equation (2.33), may be rearranged to

$$\omega^{(1)}(\alpha,\beta) = \frac{1}{\beta\pi} \int_{-2}^{+2} \sigma^{(1)}(\tau)\, F\left(\frac{\alpha-\tau}{2\delta}, \frac{\beta}{2\delta}\right) d\tau , \qquad (7.1)$$

where $F\left(\frac{\alpha-\tau}{2\delta}, \frac{\beta}{2\delta}\right)$ is defined by equation (2.37). This change was made because a computer program had previously been written to calculate F. The points at which the surface vorticity is known are not sufficient for the calculation of $\omega^{(1)}(\alpha,\beta)$. Hence, interpolation as described in section 5 was used to calculate $\sigma^{(1)}(\tau)$.

Except when the point α,β is near the cylinder surface, the calculation of the vorticity presents no difficulty. For the region of the α,β plane where $\omega^{(1)}$ is easily computed, the 40-point Gauss-Legendre formula with subintervals is applied. When $\beta \leq 0.05$ and $|\alpha| \leq$ about 2.02 the behavior of the function F must be more closely investigated, and the evaluation of the

vorticity is more complex - although some variable transformations make the integration easier than it would otherwise be.

$\omega^{(1)}(\alpha,\beta)$ was computed at the points of a rectangular mesh in the α,β plane. Next the values of α and β corresponding to constant values of $\omega^{(1)}$ were computed by using Newton's forward interpolation formula. Figure 5 shows the resulting contours in the x,y plane. To transform the values of $\omega^{(1)}$ to the x,y plane, equations (2.16), (2.17) and (2.19) are used.

8. Stream Function for the First Perturbation

Since $\omega^{(1)}(a,b)$ is odd in b and $h^2(a,b)$ is even in b, equation (2.34) may be changed to

$$\psi^{(1)}(\alpha,\beta) = -\frac{1}{2\pi}\int_0^{\infty}\int_{-\infty}^{+\infty}\frac{\omega^{(1)}(a,b)}{h^2(a,b)}\,\ln\sqrt{\frac{(\alpha-a)^2+(\beta-b)^2}{(\alpha-a)^2+(\beta+b)^2}}\,da\,db. \quad (8.1)$$

This equation could be used for calculating $\psi^{(1)}$, but it would not be an easy matter because the region of integration is the entire upper half plane and the integrand has a logarithmic singularity at $a = \alpha$, $b = \beta$. Instead, we numerically solve equation (2.26) for $n = 1$. The equation is

$$h^2\left(\frac{\partial^2\psi^{(1)}}{\partial\alpha^2}+\frac{\partial^2\psi^{(1)}}{\partial\beta^2}\right) = -\omega^{(1)}, \quad (8.2)$$

with boundary conditions

$$\psi^{(1)} = 0 \text{ at } \beta = 0$$

$$\frac{\partial\psi^{(1)}}{\partial\alpha}\to 0,\ \frac{\partial\psi^{(1)}}{\partial\beta}\to 0 \text{ as } \alpha^2+\beta^2\to\infty.$$

Equation (8.2) is not coupled with equation (2.25) because $\omega^{(1)}$ is now known. The equation pertains to the upper half of the α,β plane.

In the x,y plane equation (8.2) has the form

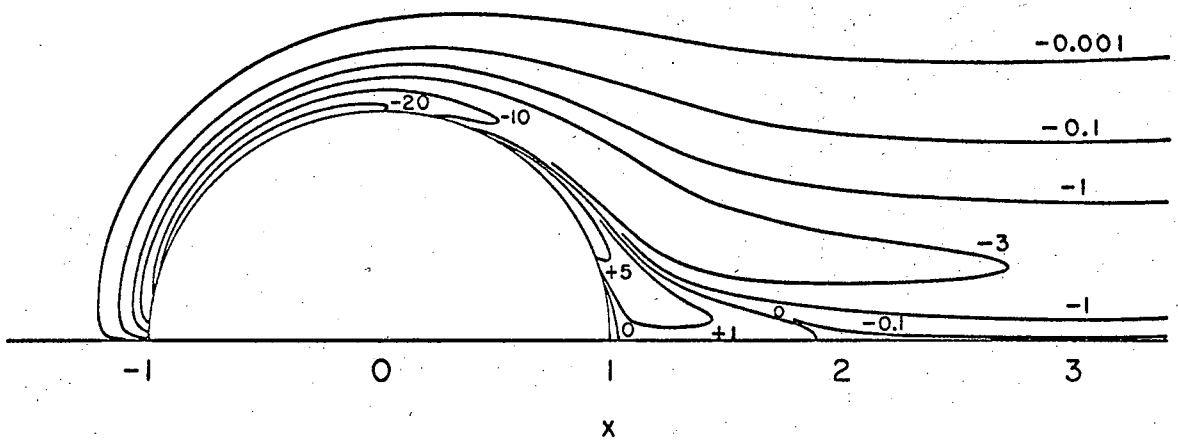

Figure 5. Vorticity for the first perturbation at a Reynolds number of 300.

$$\frac{\partial^2 \psi^{(1)}}{\partial x^2} + \frac{\partial^2 \psi^{(1)}}{\partial y^2} = - \omega^{(1)}, \tag{8.3}$$

where the boundary conditions are

$$\psi^{(1)} = 0 \text{ on the cylinder surface}$$

$$\psi^{(1)} = 0 \text{ for } |x| > 1,\ y = 0$$

$$\frac{\partial \psi^{(1)}}{\partial x} \to 0,\ \frac{\partial \psi^{(1)}}{\partial y} \to 0 \text{ as } x^2 + y^2 \to \infty .$$

Let us now transform to the ζ plane, where

$$\left.\begin{aligned} &\zeta = \ln z = \ln r + i\theta \\ &z = x + iy = r\, e^{i\theta} \\ &\zeta = \xi + i\phi, \text{ and} \\ &i = \sqrt{-1} . \end{aligned}\right\} \tag{8.4}$$

Now $\psi^{(1)}$ satisfies the equation and boundary conditions,

$$\frac{\partial^2 \psi^{(1)}}{\partial \xi^2} + \frac{\partial^2 \psi^{(1)}}{\partial \theta^2} = -e^{2\xi}\, \omega^{(1)} , \tag{8.5}$$

$$\psi^{(1)} = 0 \text{ at } \xi = 0,$$

$$\psi^{(1)} = 0 \text{ at } \theta = 0,$$

$$\psi^{(1)} = 0 \text{ at } \theta = \pi,$$

$$\frac{1}{e^{\xi}} \frac{\partial \psi^{(1)}}{\partial \xi} \to 0 \text{ as } \xi \to \infty .$$

From (8.4), it is evident that $\xi = \ln r$ and $\phi = \theta$. Thus in these coordinates, the cylinder surface in the upper half of the x,y plane is a straight line at $\xi = 0$ with the front stagnation point at $\theta = \pi$ and the rear stagnation point at $\theta = 0$. Apelt has used a similar transformation for his work at a Reynolds number of 40.

The primary advantage of the new coordinate system is that a uniform mesh size in the ξ direction corresponds to an increasingly larger mesh

size in the r direction as r gets large.

In numerical computation, one must work with a domain of finite size so the boundary condition at infinity must be set at a finite value of ξ. Thus

$$\frac{\partial \psi^{(1)}}{\partial \xi} = 0, \text{ at } \xi = \xi_{max} . \tag{8.6}$$

The problem was then solved several times for increasing values of ξ_{max} until the values of $\psi^{(1)}$ showed no appreciable change near the cylinder and in the wake.

In the θ direction, 41 mesh points were used. The mesh size, h_{θ_1}, for $0 \le \theta \le \frac{\pi}{4}$ was 1/3 the mesh size, h_{θ_2}, for $\frac{\pi}{4} \le \theta \le \pi$. This smaller mesh size was used downstream of the cylinder so that more detail could be obtained in the wake region. The mesh length chosen for the ξ direction was $h_\xi = 0.05$. The number of mesh points in the ξ direction then varies with the value of ξ_{max}.

The successive-overrelaxation method was used in solving the equations that result from approximating the derivatives in equation (8.5) by finite differences to $O(h^2)$. The equation used at the mesh points is

$$\psi_{i,j}^{(1,n+1)} = \psi_{i,j}^{(1,n)} + \frac{\Omega}{4}\left\{\frac{2p^2}{1+p^2}\left[\psi_{i+1,j}^{(1,n+1)} + \psi_{i-k,j}^{(1,n)}\right] + \frac{2}{1+p^2}\left[\Gamma + \psi_{i,j-1}^{(1,n+1)}\right] - 4\psi_{i,j}^{(1,n)} + \frac{2h_\xi^2}{1+p^2} e^{2(j-1)h_\xi} \omega_{i,j}^{(1)}\right\}, \tag{8.7}$$

where $\psi_{i,j}^{(1,n+1)}$ is the value of $\psi^{(1)}$ after the (n+1)st iteration at the point $\theta = (i-1)h_{\theta_1}$ (or $\frac{\pi}{4} + (i-21)h_{\theta_2}$ for $i > 21$) and $\xi = (j-1)h_\xi$,

$\omega_{i,j}^{(1)}$ is the value of the vorticity for the first perturbation at the point i, j,

Ω is the overrelaxation factor,

$p = h_\xi / h_{\theta_1}$ for $2 \le i \le 20$,

$p = h_\xi / h_{\theta_2}$ for $21 \le i \le 40$,

$k = 3$ for $i = 21$,

$k = 1$ for all other values of i,

$\Gamma = \psi_{i,j+1}^{(1,n)}$ for $\xi < \xi_{max}$, and

$\Gamma = \psi_{i,j-1}^{(i,n+1)}$ for $\xi = \xi_{max}$. (This accounts for the boundary conditions at $\xi = \xi_{max}$.)

The value of Ω used ranged from 1.84 to 1.96 depending on the value of ξ_{max}.

Initially, the boundary conditions at $\xi = 0$, $\theta = 0$ and $\theta = \pi$ are set. Then $\psi^{(1)}$ is set equal to zero at the remaining mesh points. Next the points along the line $j=2$ are swept by setting successively $i=40$, $i=39$, . . . $i=2$ in equation (8.7). This process is repeated for $j=3$, etc., until the whole domain has been swept. The process is then repeated until $\psi^{(1)}$ is computed to the desired accuracy. The error criterion used is

$$\left|\psi_{i,j}^{(1,n+1)} - \psi_{i,j}^{(1,n)}\right| \le 1 \times 10^{-4} \left|\psi_{i,j}^{(1,n+1)}\right|$$

for all mesh points. This procedure was then repeated for larger values of ξ_{max} until the values of $\psi^{(1)}$ showed no significant change in the region of interest. The final value of ξ_{max} used was 6 which corresponds to $r = 403$.

Perhaps one should obtain an estimate of the error involved, in replacing equation (8.5) by finite differences, by decreasing the mesh size. This was not done because it leads to a prohibitively large number of equations and it was felt that the increased computer time was not warranted.

Now that $\psi^{(1)}$ is known, the sum $\beta + \psi^{(1)}$ is found at each mesh point.

This sum is then the approximation to the stream function for $\epsilon = 1$ using the zero and first perturbations. Using Newton's forward formula for inverse interpolation, as described by Lapidus[7], contours of $\beta + \psi^{(1)}$ were computed in the ξ, θ plane. These curves were then transformed to the x,y plane to obtain Figure 6.

9. Discussion of Results

It should be mentioned that the computation time for this solution was lengthy. This is primarily because the kernel, equation (2.36), is difficult to evaluate. In the solution of equation (2.35) for $\sigma^{(1)}(\alpha)$, the evaluation of $K(\alpha,\tau)$ at the required points took about 7 hours on the IBM 7094 and CDC 6600 computers. The rest of the computation took about 1 hour on the CDC 6600.

Newman[9] has used approximate forms of the kernel which are more easily calculated. His results for the drag coefficient and pressure correction at Re = 300 are $m^{(1)} = 0.8105$ and $P^{(1)}(2,0) = -3.181$. Using the exact kernel, we obtain $m^{(1)} = 0.7070$ and $P^{(1)}(2,0) = 2.192$.

Grove[3] has studied flows which are stabilized by the placement of a splitter plate on the rear stagnation streamline. He found the dimensionless pressure at the rear stagnation point is about constant at -0.5 for $25 < Re < 300$. Using the zero and first perturbations we obtain $P(2,0) = -1.192$ for $\epsilon = 1$.

For the case of no slip on the cylinder surface it is interesting to approximate ω and ψ by the zero and first perturbations. Then $\omega = \omega^{(1)}$ and $\psi = \beta + \psi^{(1)}$.

The surface vorticity, Figure 4, has a region of negative vorticity near the rear stagnation point. This results in a secondary vortex which

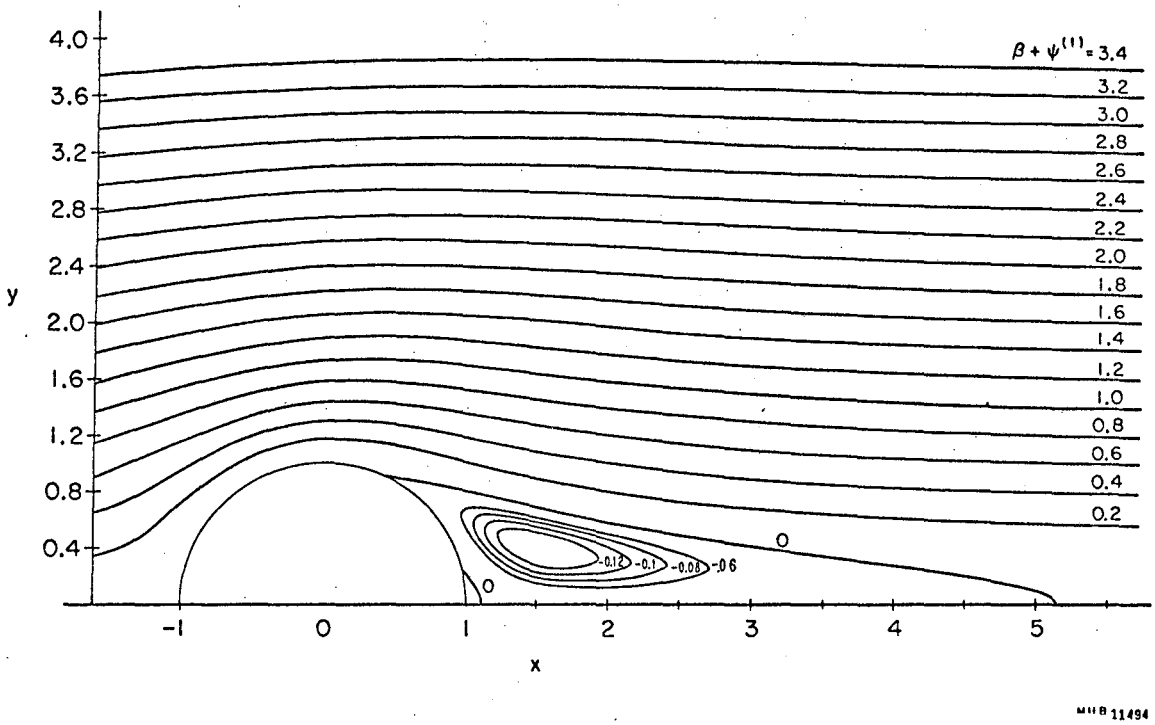

Figure 6. $\beta + \psi^{(1)}$, stream function as given by the first two terms in the perturbation series, for a Reynolds number of 300.

is visible in Figures 5 and 6.

From Figure 6, the wake stagnation point occurs at $r = 5.14$, and the point of separation is $\theta = 66°$. Grove has obtained the location of the wake stagnation point as $r = 10.2$ at $Re = 270$. The corresponding separation point is at $\theta = 72°$. Using relaxation methods Allen and Southwell[1] have obtained much smaller values for the wake stagnation point. They obtain $r = 1.9$ at $Re = 100$ and a smaller value for $Re = 1000$. The results of Allen and Southwell have been questioned by Apelt[2] and Kawaguti[5].

From the experimental results of Grove and the numerical solutions for $Re < 40$, it appears that the thickness of the wake, as shown in Figure 6, is too thin.

Evidently, more terms of the perturbation series are needed to describe the flow accurately.

Acknowledgment

This work was supported by the United States Atomic Energy Commission.

Nomenclature

a, A, b, B, C, D	- integration variables
D	- drag per unit length
D	- function arising in solution of integral equation
f	- terms in vorticity equation
F	- function in integrand of the kernel
G	- integrand of kernel in section 4
g	- function arising in solution of integral equation
h	- mesh length
h^2	- square of magnitude of potential flow velocity
H	- weight coefficients for 40-point Gauss-Legendre quadrature formula
k	- parameter in equation (8.7)
K	- kernel of integral equation
K	- modified Bessel function of second kind
ℓ	- subinterval length
m	- drag coefficient
n	- number of subintervals
p	- parameter in equation (8.7)
p	- pressure
p_∞	pressure far from the cylinder
P	- dimensionless pressure
r^*	- distance from the cylinder center
r	- dimensionless distance from the cylinder center
R	- radius of the cylinder
Re	- Reynolds number

$\mathrm{sgn}(\eta)$ - sign (+1 or -1) of η

U - uniform velocity far from the cylinder

v_x^* - velocity in the x^* direction

v_y^* - velocity in the y^* direction

x^*, y^* - rectangular coordinates

x, y - dimensionless rectangular coordinates

z - complex variable = $x + i\,y$

z - nodes of 40-point Gauss-Legendre quadrature formula

α - velocity potential for the ideal flow

β - stream function for the ideal flow

Γ - parameter in equation (8.7)

δ - $2/\mathrm{Re} = \nu/UR$

ϵ - perturbation parameter

ζ - complex variable = $\xi + i\,\phi$

η - $(\alpha-\tau)/2\delta$

θ - angle measured in the counterclockwise direction from the rear stagnation point of the cylinder

ν - kinematic viscosity of the fluid

ξ_1, ξ_2 - $\frac{2+\alpha}{2\delta}$, $\frac{2-\alpha}{2\delta}$ used in equation (5.4)

ξ - coordinate = $\ln r$

ρ - fluid density

σ - surface vorticity

τ - integration variable

ϕ - same as θ

χ - function arising in solution of integral equation

ψ^* - stream function

ψ - dimensionless stream function

ω^* - vorticity

ω - dimensionless vorticity

Ω - overrelaxation factor

$(0),(1),\ldots,(n)$ - superscripts denoting order of the perturbation

$(1,n),(1,n+1)$ - superscripts on ψ denoting (order of perturbation, iteration number)

References

1. Allen, D. N. de G., and R. V. Southwell, "Relaxation Methods Applied to Determine the Motion in Two Dimensions of a Viscous Fluid Past a Fixed Cylinder," Quart. J. Mech. Appl. Math., 8, 129 (1955).

2. Apelt, C. J., Some Studies of Fluid Flow at Low Reynolds Numbers, Dissertation, University of Oxford, 1957.

3. Grove, Andrew S., An Investigation into the Nature of Steady Separated Flows at Large Reynolds Numbers, Dissertation, University of California, Berkeley, 1963.

4. Kantorovich, L. V., and V. I. Krylov, Approximate Methods of Higher Analysis (Interscience Publishers, Inc., New York, Translated by Curtis D. Benster, 1959).

5. Kawaguti, Mitutosi, "Note on Allen and Southwell's paper 'Relaxation Methods Applied to Determine the Motion, in Two Dimensions, of a Viscous Fluid Past a Fixed Cylinder'," Quart. J. Mech. Appl. Math., 12, 261 (1959).

6. Krylov, V. I., Approximate Calculation of Integrals (The MacMillan Company, New York, Translated by Arthur H. Stroud, 1962).

7. Lapidus, L., Digital Computation for Chemical Engineers (McGraw-Hill Book Co., Inc., New York, 1962).

8. McDonald, Marvin E., Numerical Calculation for the Steady Laminar Flow Past a Circular Cylinder, Master's Thesis, University of California, Berkeley, 1966.

9. Newman, John S., Steady Laminar Flow past a Circular Cylinder at High Reynolds Numbers, Dissertation, University of California, Berkeley, 1963.

10. Sih, P. H., Numerical Computation of Flow Past Obstacles, Master's Thesis, University of California, Berkeley, 1966.

11. Southwell, R. V. and H. B. Squire, "A Modification of Oseen's Approximate Equation for the Motion in Two Dimensions of a Viscous Incompressible Fluid," Phil. Trans. Roy. Soc., London, A232, 27 (1933).